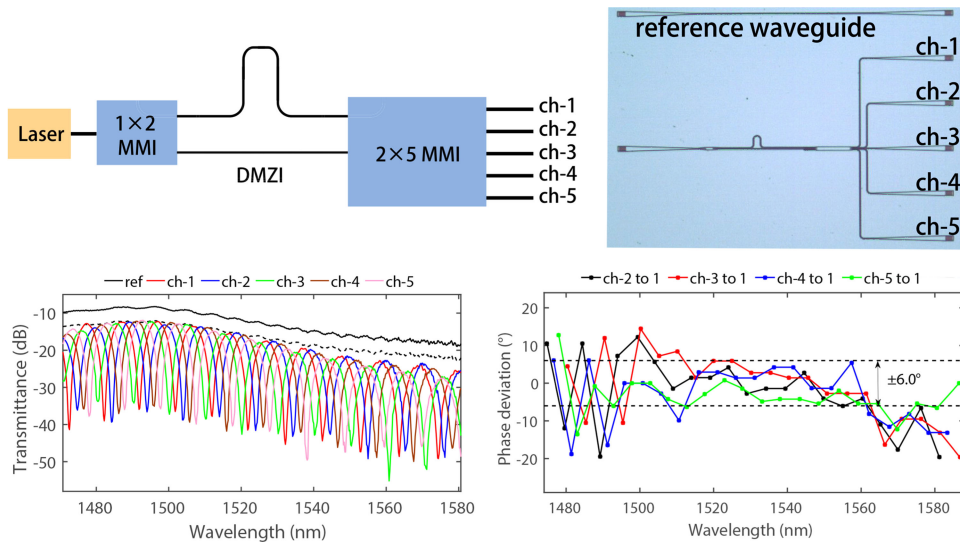


Compact Low-Loss Optical 72° Hybrid Based on Nonoverlapping-Image Multimode Interference Coupler in Silicon-on-Insulator

Volume 11, Number 6, December 2019

Zezheng Li
Yingxin Kuang
Huan Guan
Yang Liu
Xinqun Zhang
Weihua Han
Zhiyong Li



DOI: 10.1109/JPHOT.2019.2956260

Compact Low-Loss Optical 72° Hybrid Based on Nonoverlapping-Image Multimode Interference Coupler in Silicon-on-Insulator

Zezheng Li ,^{1,2} Yingxin Kuang ,^{1,2} Huan Guan ,² Yang Liu ,^{1,2} Xinqun Zhang,² Weihua Han,² and Zhiyong Li²

¹College of Materials Science and Opto-Electronic Technology, University of Chinese Academy of Sciences, Chinese Academy of Sciences, Beijing 100049, China

²State Key Laboratory on Integrated Optoelectronics, Institute of Semiconductors, Chinese Academy of Sciences, Beijing 100083, China

DOI:10.1109/JPHOT.2019.2956260

This work is licensed under a Creative Commons Attribution 4.0 License. For more information, see <https://creativecommons.org/licenses/by/4.0/>

Manuscript received September 10, 2019; revised November 15, 2019; accepted November 22, 2019. This work was supported in part by the National Key Research and Development Plan of China under Grant 2018YFB2200202 and in part by the National Natural Science Foundation of China under Grant 61804148. Corresponding author: Zhiyong Li (e-mail: lizhy@semi.ac.cn).

Abstract: A universal principle to achieve different optical hybrids is summarized based on general nonoverlapping-image MMI couplers. An optical 72° hybrid is proposed and demonstrated which is achieved by a 2 × 5 multimode interference (MMI) coupler with length of 89.5 μm and width of 8.0 μm . The device is fabricated in silicon-on-insulator (SOI) with 220 nm thick top silicon layer and the buried oxide layer is 3 μm thick. The proposed device exhibits an extinction ratio larger than 20 dB from 1470.8 nm to 1581.2 nm. The excess loss of optical hybrid is about 1.4 dB and a phase deviation less than $\pm 6.0^\circ$ is obtained with the bandwidth of 51.5 nm.

Index Terms: Integrated optics, multimode interference coupler, silicon-on-insulator, optical hybrid.

1. Introduction

Multimode interference (MMI) coupler is a kind of multi-port optical structure which performs the basic function of beam splitting and combining. Light input from any port will excite several modes with different propagation constant. One or more images of the input light field appear at different lateral direction when multi-modes propagate through the region of coupler. Some theoretical aspects have been developed [1]–[6] to describe the optical behavior of light in MMI couplers so far. Many complex optical devices based on MMI couplers have been investigated such as switches [7], [8], sensors [9], [10], routers [11], [12] and optical hybrids [13]–[18].

The optical hybrid is a kind of advanced device which is central to many applications such as coherent transmission systems [19] and phase sensitive detection [20], [21], which can be achieved by MMI couplers. Generally, the MMI couplers applied for the hybrid should provide certain relative phase difference at different output ports when light is incident from different input ports [22], [23]. In this paper, the optical phase matrix of general nonoverlapping-image MMI coupler is analyzed with the deduction of important phase principles. The relation between phase matrix and image's

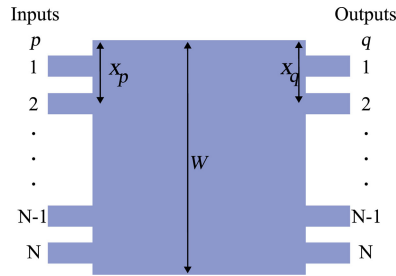


Fig. 1. Schematic view of general nonoverlapping-image MMI coupler with N input and output ports. The positions of input and output ports are determined by $x_p = (p - 0.5)W/N$, $x_q = (q - 0.5)W/N$ with $p, q = 1, 2 \dots N$.

relative phase information is interpreted, which is instructive to design hybrid with different degrees. The physical significance and principles obtained from the phase relation is summarized with key parameters. Based on the presented principle of optical hybrids, we proposed three kinds of 72° optical hybrids based on 5×5 nonoverlapping-image MMI coupler. We fabricate the hybrid with the best simulated characteristic. Experimental result shows that the device exhibits an extinction ratio larger than 20 dB with the bandwidth of 110 nm which covers C-band spectra range. The insertion loss of hybrid is less than 1.4 dB for the best wavelength range and a phase deviation less than 6.0° is obtained within the bandwidth of 51.5 nm. The fabricated device is based on 220-nm silicon-on-insulator (SOI) platform and the testing results are well matching the simulated characteristic.

2. Analysis of Phase Principles

The general nonoverlapping-image MMI coupler is shown in Fig. 1. According to Ref. 4, the self-image's phase information of nonoverlapping-image MMI coupler is

$$\varphi_{q,p} = \phi_1 - \frac{\pi}{2}(-1)^{q+p+N} + \frac{\pi}{4N} \times \left[q + p - q^2 - p^2 + (-1)^{q+p+N} \left(2qp - q - p + \frac{1}{2} \right) \right] \quad (1)$$

For a specified MMI coupler, when incident light from two different input ports propagate to the same output ports, the phase difference between them is important for the requirement of optical hybrid. According to Eq. (1),

$$\begin{aligned} \varphi_{j,m} - \varphi_{j,n} = & -\frac{\pi}{2} [(-1)^{m+j+N} - (-1)^{n+j+N}] + \frac{\pi}{4N} \times \left[m + n - m^2 + n^2 \right. \\ & \left. + (-1)^{m+j+N} \left(2mj - m - j + \frac{1}{2} \right) - (-1)^{n+j+N} \left(2nj - n - j + \frac{1}{2} \right) \right] \end{aligned} \quad (2)$$

where m and n denote two input ports and j is a changing index which can go through 1 to N . Here consider two cases based on the parity of $m - n$ and assume $m > n$ in the following discussion.

2.1 $m - n$ Is Even

When $m - n$ is even, define $m - n = 2a$ and a can be 1, 2, 3.... Here $(-1)^{m+j+N} - (-1)^{n+j+N}$ must be zero and

$$\begin{aligned} \varphi_{j,m} - \varphi_{j,n} = & \frac{\pi}{4N} \times \left[m + n - m^2 + n^2 + (-1)^{m+j+N} \left(2mj - m - j + \frac{1}{2} - 2nj + n + j - \frac{1}{2} \right) \right] \\ = & \frac{\pi}{4N} \times [2a - 4am + 4a^2 + (-1)^{m+j+N} (4aj - 2a)] \end{aligned} \quad (3)$$

In above equation, the value of $(-1)^{m+j+N}$ is 1 for the case of $m + j + N$ is even and -1 for the case of $m + j + N$ is odd. Its noted that for a certain MMI coupler, N is first determined regardless of odd or even. Then index j can be chosen from 1 to N . When j increases from 1 to N , the value of $(-1)^{m+j+N}$ is 1 and -1 alternately so a further classification is needed based on the parity of $m + j + N$ and j .

2.1.1 $m + j + N$ Is Even When j Is Odd: Here $m + j + N$ is even when j is odd, so $m + j + N$ is odd when j is even. We can classify $\varphi_{j,m} - \varphi_{j,n}$ expressed by Eq. (3) into two numerical series:

$$\varphi_{j,m} - \varphi_{j,n} = \frac{\pi a}{N}(a + j - m) \Big|_{j=1,3,5,\dots} \quad \varphi_{j,m} - \varphi_{j,n} = \frac{\pi a}{N}(a - j - m + 1) \Big|_{j=2,4,6,\dots} \quad (4)$$

Its clear that both of the two series are arithmetic progressions. When index j is changed by 2, $\varphi_{j,m} - \varphi_{j,n}$ is changed by $2\pi a/N$ correspondingly. Here we define the difference of series elements as $\Delta\varphi = 2\pi a/N$. Furthermore, careful analysis shows that

$$\frac{\pi a}{N}(a + j - m) \Big|_{j=1} - \frac{\pi a}{N}(a - j - m + 1) \Big|_{j=2} = \frac{2\pi a}{N} = \Delta\varphi \quad (5)$$

Above equation indicates that the minimum term in series $\frac{\pi a}{N}(a + j - m) \Big|_{j=1,3,5,\dots}$ is larger than the maximum term in series $\frac{\pi a}{N}(a - j - m + 1) \Big|_{j=2,4,6,\dots}$ by $\Delta\varphi = 2\pi a/N$. So we can combine the two series into a uniform series with number of terms N and arithmetic progression value of $\Delta\varphi = 2\pi a/N$.

2.1.2 $m + j + N$ Is Odd When j Is Odd: For this case, a similar classification can be done for the phase difference $\varphi_{j,m} - \varphi_{j,n}$:

$$\varphi_{j,m} - \varphi_{j,n} = \frac{\pi a}{N}(a - j - m + 1) \Big|_{j=1,3,5,\dots} \quad \varphi_{j,m} - \varphi_{j,n} = \frac{\pi a}{N}(a + j - m) \Big|_{j=2,4,6,\dots} \quad (6)$$

Compared with Eq. (4), both of the above two series are also arithmetic progressions with the same changing relation of $\varphi_{j,m} - \varphi_{j,n}$ related to index j . Here the key relation of two series is:

$$\frac{\pi a}{N}(a + j - m) \Big|_{j=2} - \frac{\pi a}{N}(a - j - m + 1) \Big|_{j=1} = \frac{2\pi a}{N} = \Delta\varphi \quad (7)$$

It is noted that this principle is equivalent to Eq. (5) so the two series for this case can also be written by a uniform expression and the arithmetic progression value is still $\Delta\varphi = 2\pi a/N$.

2.2 $m - n$ Is Odd

When $m - n$ is odd, define $m - n = 2a + 1$ and a can be 0, 1, 2, ... The sign of $(-1)^{m+j+N}$ and $(-1)^{n+j+N}$ must be different. Then the phase difference can be written as

$$\varphi_{j,m} - \varphi_{j,n} = (-1)^{m+j+N+1}\pi + \frac{\pi}{2N} \times \{(m - a - 1)[(-1 - 2a) + (-1)^{m+j+N}(2j - 1)]\} \quad (8)$$

Here we can make a similar discussion based on the parity of $m + j + N$ with j and arrive at another principle.

2.2.1 $m + j + N$ Is Even When j Is Odd:

$$\begin{aligned} \varphi_{j,m} - \varphi_{j,n} &= -\pi + \frac{\pi}{N}(m - a - 1)(-1 - a + j) \Big|_{j=1,3,5,\dots} \\ \varphi_{j,m} - \varphi_{j,n} &= \pi + \frac{\pi}{N}(m - a - 1)(-a - j) \Big|_{j=2,4,6,\dots} \end{aligned} \quad (9)$$

Both of the above two series are arithmetic progressions. Here when index j is changed by 2, $\varphi_{j,m} - \varphi_{j,n}$ is changed by $\Delta\varphi = 2\pi(m - a - 1)/N$, which is different from the result of part 2.1. Furthermore, careful analysis shows that

$$\frac{\pi(m - a - 1)}{N}(-1 - a + j) \Big|_{j=1} - \frac{\pi(m - a - 1)}{N}(-a - j) \Big|_{j=2} = \frac{2\pi(m - a - 1)}{N} = \Delta\varphi \quad (10)$$

TABLE 1
Principle of Phase-Related Parameters Based on Nonoverlapping Image MMI Coupler

$m - n$	$P_{m+j+N} \neq P_j$	$P_{m+j+N} = P_j$	$\Delta\varphi$
$2a$	$j \uparrow, \varphi_{j,m} - \varphi_{j,n} \uparrow$	$j \uparrow, \varphi_{j,m} - \varphi_{j,n} \downarrow$	$2\pi a/N$
$2a + 1$	$j \uparrow, \varphi_{j,m} - \varphi_{j,n} \uparrow$	$j \uparrow, \varphi_{j,m} - \varphi_{j,n} \downarrow$	$2\pi(m - a - 1)/N$

It is noted that the term of $-\pi - \pi = -2\pi$ is omitted in the above equation which has no impact on the physical significance of phase difference so the phase difference $\varphi_{j,m} - \varphi_{j,n}$ can still be written as a uniform series while the difference value of adjacent two terms is $2\pi(m - a - 1)/N$. Analogical discussion can be done for the case of $m + j + N$ is odd when j is odd and arrive at the conclusion that $\varphi_{j,m} - \varphi_{j,n}$ can be combined into a complete series so we omit the deduction process here.

Above all, the parity of $m + j + N$ and j can be denoted as P_{m+j+N} and P_j which can be odd or even. For the case of $P_{m+j+N} \neq P_j$, when index j increases, the phase series $\varphi_{j,m} - \varphi_{j,n}$ increases. For the case of $P_{m+j+N} = P_j$, when j increases, $\varphi_{j,m} - \varphi_{j,n}$ decreases. Its change relation corresponding to index j is decided by the parity of $m + j + N$. We summary these principles in Table 1.

In the above analysis, the principle of relative phase difference $\Delta\varphi$ holds true for any nonoverlapping image MMI couplers. Physically, the phase element $\varphi_{j,m}$ corresponds to the relative phase change when light propagates through the coupler from input port m to output port j . The phase progressions physical significance $(\varphi_{j,m} - \varphi_{j,n})$ represents the law of two images relative phase difference at different output ports when light is input from two different input ports of the MMI coupler, which is the vital information for the design of different hybrids. For example, the optical 72° hybrid requires that when light is input from two different ports, the corresponding image-light's relative phase difference $\varphi_{j,m} - \varphi_{j,n}$ at different output ports should be 0, 72°, 144°, 216° and 288°.

3. Discussion and Simulation of Optical 72° Hybrid

According to the principle summarized in table 1, optical 72° hybrids can be achieved based on the nonoverlapping-image MMI couplers and the key issue is to determine the important parameters of $\Delta\varphi$, N , a , m and n in order. For a 72° hybrid, the condition is $\Delta\varphi = 2\pi/5$.

For $m - n = 2a$, let $2\pi a/N = 2\pi/5$ and $N = 5a$. Because N and a must be positive integers, the minimum possible value of N is $N = 5a = 5$, which represents 5 × 5 MMI coupler. Here $2a = 2$ so the difference of two input port number is 2. The corresponding solutions of the port index for two input light are 1 and 3, 2 and 4, 3 and 5. So there are three solutions for 72° hybrid based on the 5 × 5 nonoverlapping-image MMI coupler when $m - n$ is even.

For the case of $m - n = 2a + 1$, let $2\pi(m - a - 1)/N = 2\pi/5$ and $N = 5(m - a - 1)$. Because $0 < m - a - 1 < N$, the minimum possible value of N is still 5, which also represents the MMI coupler with five input/output ports. Here $m - a = 2$, if a takes the minimum possible value of 0, then m is 2 and n is 1, which is a reasonable solution. When a increases, its clear that no solution of m and n can be found for the limitation of $1 \leq n < m < 5$. For this case, there is only one reasonable configuration of input light and relative phase difference of output ports.

In fact, scheme $n = 1, m = 3$ is equivalent to scheme $n = 3, m = 5$ based on the symmetry of coupler so there are actually three different schemes of 72° hybrid based on the 5 × 5 nonoverlapping-image MMI coupler. We optimized the coupler based on 220-nm SOI by a three-dimensional finite-difference time-domain (3D-FDTD) solver. For the 5 × 5 MMI coupler, the width and length are 8.0 μm and 89.5 μm respectively.

The simulated phase deviation for the three kinds of hybrid is shown in Fig. 2 where the phase difference of output port 1 is chosen as the referenced value. Because the phase difference for the five output ports are integral multiple of 72°, the simulated results from output port 2 to output port 5 are normalized to 72° by subtracting certain multiple of 72°. As clearly seen for hybrids with

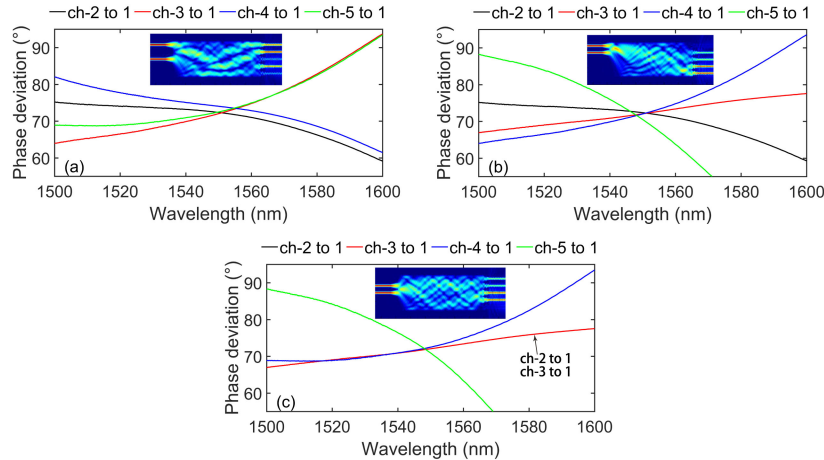


Fig. 2. Simulated phase deviation of 72° hybrid with (a) $n = 1$, $m = 3$, (b) $n = 1$, $m = 2$ and (c) $n = 2$, $m = 4$. The inserted optical light profile shows the optical propagation state of two input signals without phase difference for the three kinds of hybrid.

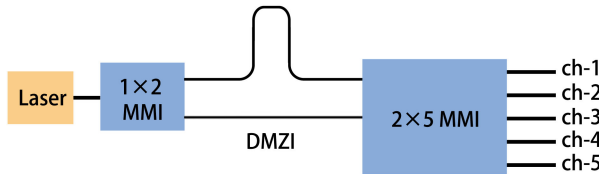


Fig. 3. Schematic drawing of the fabricated device for the test of optical 72° hybrid with the configuration of $n = 1$ and $m = 3$.

$n = 1$, $m = 3$ and $n = 1$, $m = 2$, two deviation lines go up when lambda shifts to long wavelength region while the other two lines go down. The four lines of two kinds of hybrid converge near the region of the center of C-band which has the best value about 72°. It is noted that there are two lines coinciding with each other in the hybrid with $n = 2$, $m = 4$ which is present in Fig. 2(c). For these three hybrids, the simulated bandwidths within the $72 \pm 6^\circ$ phase deviation are 51.8 nm, 35.2 nm and 26.8 nm respectively. In the long wavelength region near 1600 nm, simulation result shows that the phase characteristic is deteriorated because of the self-image's mismatch of MMI coupler.

4. Fabrication and Experimental Results

According to the simulation for the three types of 72° hybrids, the five output port's phase performance of configuration with $n = 1$, $m = 3$ is better than that of configurations with $n = 1$, $m = 2$ and $n = 2$, $m = 4$. So we choose the best hybrid with $n = 1$, $m = 3$ to fabricate devices. Based on the Eq. (2), when two signals are input from the first and third input port of 5×5 MMI coupler, the phase difference of two signals at five output ports are 0, 72°, 288°, 144° and 216° respectively, which actually satisfied the requirement of 72° hybrid. This kind of hybrid is renamed as n1m3 72° hybrid in the following sections. Fig. 3 is the structure of the fabricated device.

A 1×2 MMI coupler is the first stage splitter to achieve two signals with equal magnitude. Then a delayed Mach-Zehnder interferometer (DMZI) is used to form a specified free spectral range (FSR) within the measured spectrum. The output ports of DMZI are connected to the two corresponding input ports of 5×5 MMI coupler for the n1m3 hybrid. The device is fabricated on SOI with 220-nm thick top-silicon layer for the full-etching condition. The width of single-mode waveguide is 500 nm.

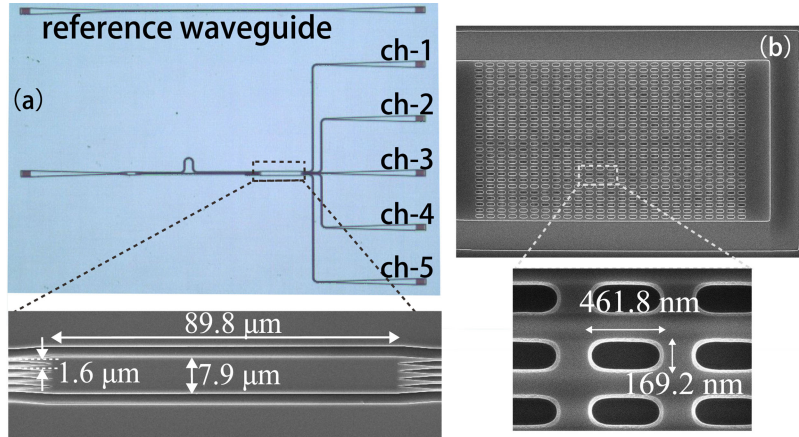


Fig. 4. (a) The microscope view of the fabricated 72° hybrid and scanning electron microscope (SEM) view of the MMI coupler, (b) SEM view of the sub-wavelength grating coupler. The designed size of etching element is 445 nm × 171 nm.

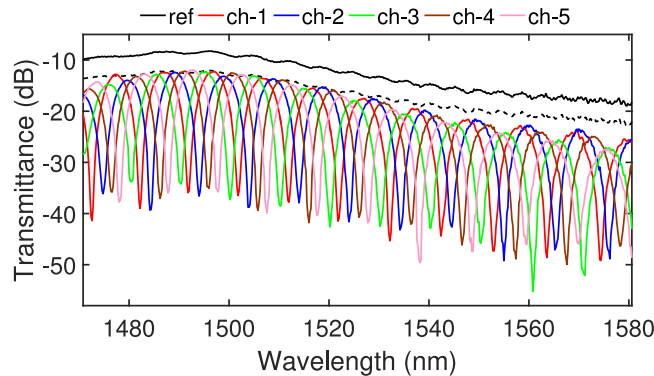


Fig. 5. Measured transmission spectra of n1m3 72° hybrid. The transmittance of referenced waveguide is plotted which shows the spectra of sub-wavelength grating coupler. The black dashed line is a referenced line in which the equivalent virtual loss has been excluded.

As to our optimization by 3D-FDTD method, the width and length of the 1×2 MMI coupler are $4.8 \mu\text{m}$ and $19.5 \mu\text{m}$. The DMZI's length difference is designed as $54.8 \mu\text{m}$, which determines the FSR to be 10 nm .

Figure 4 shows the microscope and scanning electron microscope (SEM) views of the tested devices. Sub-wavelength grating couplers are used for the input and output ports to achieve vertical fiber coupling, which can maintain a uniform coupling efficiency within the full-etching fabrication. A light beam from a tunable laser (Yokogawa, AQ2200-136) is controlled to be a TE mode by polarization controller before coupling to the input waveguide from a single-mode fiber. A spectrometer (Yokogawa, AQ6370 C) is used to measure the output signals of five channels. Fig. 5 is the measured spectra of hybrid which covers the whole C-band.

For a 72° hybrid, the phase differences of two signals at each output port of the 5×5 MMI coupler are different, so the output power cannot be totally collected in any output port, causing an equivalent virtual loss of 3.98 dB for each output channel, which has been shown in Fig. 5. The FSR of each output signal is related to the wavelength and the experiment result shows a uniform FSR from 10.07 nm to 10.18 nm for the n1m3 72° hybrid. The spectra lines exhibit a slight vibration in the long wavelength region due to the fabrication error of sub-wavelength gratings. The n1m3 72°

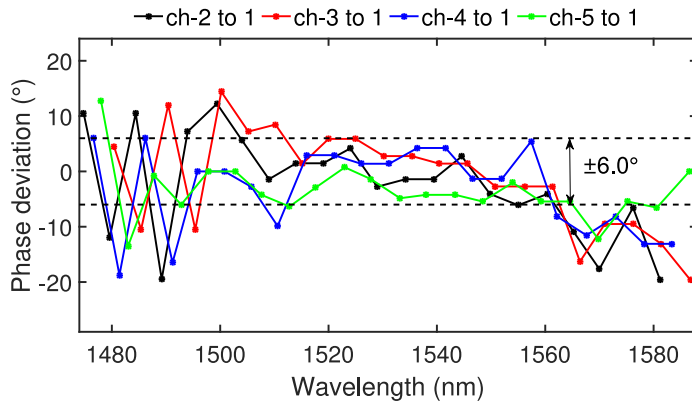


Fig. 6. Calculated phase deviation related to channel-1 of n1m3 optical 72° hybrid. The two horizontal dashed lines represent the threshold for the phase deviation of 6.0°.

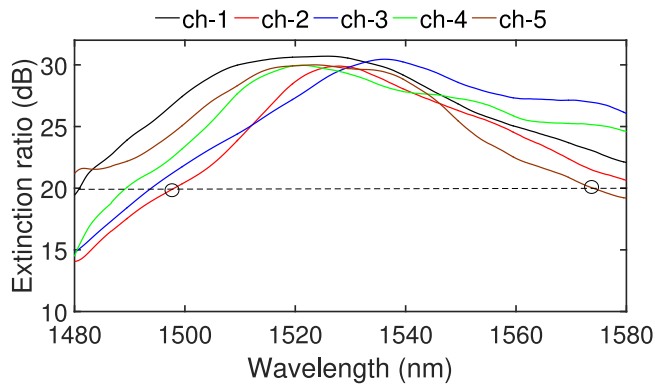


Fig. 7. Calculated extinction ratio of n1m3 72° hybrid. A single additional 5×5 MMI coupler is fabricated on chip and the transmittance from any input port to any output port can be measured to calculate the extinction ratio. The horizontal dashed line shows the value of 20-dB extinction ratio, which represents the deviation of normalized amplitude of 0.2 ± 0.02 .

hybrid exhibits an insertion loss less than 1.4 dB from 1481.6 nm to 1526.4 nm. The extinction ratio is related to the interference characteristic of hybrid. For the five output ports of n1m3 72° hybrid, we obtain a minimum extinction ratio larger than 20 dB from 1470.8 nm to 1581.2 nm, which covers the C-band spectral range. For the best output channels of 1, 2 and 5, the extinction ratio is larger than 23.7 dB over 100 nm spectra range.

The phase deviation is a typical parameter of hybrid. We calculated the phase deviation of hybrid based on the following relation: $\Delta\varphi/360 = \Delta\lambda/FSR$, where $\Delta\varphi$ is the two output signals phase change related to the theoretical value. The phase information of channel 1 is set as the referenced spectra line so FSR is chosen from every period of output port 1 which is shown in Fig. 5. The phase deviation can be obtained by calculating $\Delta\lambda$ of other four output spectra within the corresponding FSR and the result is shown in Fig. 6. The center wavelength of the best region has a slight shift from 1550 nm to the short wavelength because of the fabrication error of 2×5 MMI coupler in n1m3 72° hybrid. The device exhibits a phase deviation less than 6.0° from 1512.2 nm to 1563.7 nm and the bandwidth is 51.5 nm, well matching the simulation result in Fig. 2.

The power imbalance of 5×5 MMI coupler is another important characteristic because it influences the extinction ratio of hybrid. By testing the power of five output ports when light is incident from input port 1 and 3, we obtain the power imbalance of 5×5 MMI coupler and the calculated result of extinction ratio is shown in Fig. 7.

For every output port, the power difference of signals from two different input ports is calculated and then changed into extinction ratio. The extinction ratio of n1m3 72° hybrid is larger than 20 dB from 1500 nm to 1575 nm with the bandwidth of 75 nm. In the short wavelength region near 1480 nm, the lines of channel 2, 3 and 4 are less than 20 dB and it limits the minimum extinction ratio of hybrid, which matches the testing result of spectra in Fig. 5. It is noted that the actual extinction ratio only occurs in every FSR with one value, so the estimation here is a lower limit of extinction ratio for the hybrids, which compares well to the testing result in Fig. 5.

5. Conclusions

In this paper, we theoretically analyze the optical phase principle of general nonoverlapping-image MMI coupler for the achievement of optical hybrids. An interpretation of phase information is presented with the analog between physical significance and device function. Based on the presented principle along with key parameters, we experimentally demonstrate an optical 72° hybrid in 220-nm SOI platform. Testing result shows that the fabricated device exhibits an extinction ratio larger than 20 dB with the bandwidth of 110 nm, an excess loss of 1.4 dB within 44 nm range and a phase deviation less than 6.0° with the bandwidth of 51.5 nm. The proposed optical hybrid and phase principle here can be used for applications such as coherent transmission systems and multi-level phase-shift keying optical communications.

Acknowledgment

The authors would like to thank the anonymous reviewers for their valuable suggestions.

References

- [1] Z. C. Le, S. G. Huang, M. L. Fu, D. Wen, Z. Jie, and Z. Ming, "Study on self-imaging properties for line-tapered multimode interference couplers," *Opt. Commun.*, vol. 284, no. 22, pp. 5303–5310, 2011.
- [2] J. M. Heaton and R. M. Jenkins, "General matrix theory of self-imaging in multimode interference (MMI) couplers," *IEEE Photon. Technol. Lett.*, vol. 11, no. 2, pp. 212–214, Feb. 1999.
- [3] L. B. Soldano and E. C. M. Pennings, "Optical multi-mode interference devices based on self-imaging: Principles and applications," *J. Lightw. Technol.*, vol. 13, no. 4, pp. 615–627, Apr. 1995.
- [4] M. R. Paiam and R. I. Macdonald, "Design of phased-array wavelength division multiplexers using multimode interference couplers," *Appl. Opt.*, vol. 36, no. 21, pp. 5097–5108, 1997.
- [5] P. A. Besse, M. Bachmann, C. Nadler, and H. Melchior, "The integrated prism interpretation of multileg Mach-Zehnder interferometers based on multimode interference couplers," *Opt. Quantum Electron.*, vol. 27, no. 10, pp. 909–920, 1995.
- [6] M. Bachmann, P. A. Besse, and H. Melchior, "Overlapping-image multimode interference couplers with a reduced number of self-images for uniform and nonuniform power splitting," *Appl. Opt.*, vol. 34, no. 30, pp. 6898–6910, 1995.
- [7] S. Mu, K. Liu, S. Wang, C. Zhang, B. Guan, and D. Zou, "Compact InGaAsP/InP 3 × 3 multimode-interference coupler-based electro-optic switch," *Appl. Opt.*, vol. 55, no. 7, pp. 1795–1802, 2016.
- [8] C. D. Truong, M. C. Nguyen, D. T. Le, and T. T. Le, "All-optical switch based on 1 × 3 multimode interference couplers," *Opt. Switching Netw.*, vol. 22, no. C, pp. 129–134, 2016.
- [9] T.-T. Le, "Two-Channel highly sensitive sensors based on 4 × 4 multimode interference couplers," *Photon. Sensors*, vol. 7, no. 4, pp. 357–364, Dec. 2017.
- [10] R. Copperwhite, M. Oubaha, J. Moore, C. McDonagh, and B. D. Macraith, "Sensing performance of a refractometric optical sensor platform based on multimode interference couplers," *IEEE Sensors J.*, vol. 11, no. 12, pp. 3269–3275, Dec. 2011.
- [11] A. Cantarero, A. Crespopoveda, and M. M. D. Lima, "Reconfigurable photonic routers based on multimode interference couplers," *J. Opt. Soc. Amer. B*, vol. 33, no. 1, pp. 81–89, 2016.
- [12] J. Z. Huang, R. Scarmozzino, and R. M. Osgood, Jr, "A new design approach to large input/output number multimode interference couplers and its application to low-crosstalk WDM routers," *IEEE Photon. Technol. Lett.*, vol. 10, no. 9, pp. 1292–1294, Sep. 1998.
- [13] W. Yang, M. Yin, Y. Li, X. Wang, and Z. Wang, "Ultra-compact optical 90° hybrid based on a wedge-shaped 2 × 4 MMI coupler and a 2 × 2 MMI coupler in silicon-on-insulator," *Opt. Exp.*, vol. 21, no. 23, pp. 28 423–28 431, 2013.
- [14] J. Seok-Hwan and M. Ken, "Compact optical 90° hybrid employing a tapered 2 × 4 MMI coupler serially connected by a 2 × 2 MMI coupler," *Opt. Exp.*, vol. 18, no. 5, pp. 4275–4288, 2010.
- [15] X. Min, S. Pan, and Y. Zhao, "Optical single-sideband modulation based on a dual-drive MZM and a 120° hybrid coupler," *J. Lightw. Technol.*, vol. 32, no. 19, pp. 3317–3323, Oct. 2014.
- [16] J. S. Hwan and M. Ken, "Optical 60° hybrid for demodulating six-level DPSK signal," *Opt. Lett.*, vol. 36, no. 3, pp. 322–324, 2011.

- [17] Z. Zheng *et al.*, "Optical single sideband millimeter-wave signal generation and transmission using 120° hybrid coupler," *Opt. Commun.*, vol. 411, no. 22, pp. 21–26, Mar. 2018.
- [18] R. Uda, K. Yamaguchi, K. Takada, and K. Okamoto, "Fabrication of a silica-based complex Fourier-transform integrated-optic spatial heterodyne spectrometer incorporating 120° optical hybrid couplers," *Appl. Opt.*, vol. 57, no. 14, pp. 3781–3787, 2018.
- [19] A. Wongfoy *et al.*, "Monolithic demodulator for 40-gb/s DQPSK using a star coupler," *J. Lightw. Technol.*, vol. 24, no. 1, pp. 171–174, Jan. 2006.
- [20] L. Zimmermann, K. Voigt, G. Winzer, K. Petermann, and C. M. Weinert, "C-band optical 90°-hybrids based on silicon-on-insulator 4 × 4 waveguide couplers," *IEEE Photon. Technol. Lett.*, vol. 21, no. 3, pp. 143–145, Feb. 2009.
- [21] C. R. Doerr, L. Zhang, S. Chandrasekhar, and L. L. Buhl, "Monolithic DQPSK receiver in InP with low polarization sensitivity," *IEEE Photon. Technol. Lett.*, vol. 19, no. 21, pp. 1765–1767, Nov. 2007.
- [22] S. H. Jeong and K. Morito, "Optical 90° hybrid with broad operating bandwidth of 94 nm," *Opt. Lett.*, vol. 34, no. 22, pp. 3505–3507, 2009.
- [23] S. H. Jeong and K. Morito, "Optical 45 degrees hybrid for demodulating 8-ary DPSK signal," *Opt. Exp.*, vol. 18, no. 8, pp. 8482–90, 2010.